View metadata, citation and similar papers at core.ac.uk

brought to you by CORE

provided by CURVE/open

Microstructural degradation of Ti-45Al-8Nb alloy during the fabrication process by electron beam melting

Wenbin Kan; Yongfeng Liang; Hui Peng; Bo Chen; Hongbo Guo and Junpin Lin

Post-print deposited in Coventry University Repository

Original citation:
Kan, W; Liang, Y; Peng, H; Chen, B; Guo, H. and Lin, J. (2017) Microstructural degradation of Ti-45Al-8Nb alloy during the fabrication process by electron beam melting. *JOM Journal of the Minerals, Metals and Materials Society* (in press).

Springer

The final publication is available at link.springer.com via http://dx.doi.org/[insert DOI]

Copyright © and Moral Rights are retained by the author(s) and/ or other copyright owners. A copy can be downloaded for personal non-commercial research or study, without prior permission or charge. This item cannot be reproduced or quoted extensively from without first obtaining permission in writing from the copyright holder(s). The content must not be changed in any way or sold commercially in any format or medium without the formal permission of the copyright holders.

Manuscript
Click here to download Manuscript JOM-clean version_Kan_20170810.docx
Click here to view linked References

Microstructural degradation of Ti-45Al-8Nb alloy during the fabrication process by electron beam melting

Wenbin Kan[a], Yongfeng Liang[a,*], Hui Peng[b,c,*], Bo Chen[d], Hongbo Guo[b,c], Junpin Lin[a]

[a]*State Key Laboratory for Advanced Metals and Materials, University of Science and Technology Beijing, Beijing 100083, China*

[b]*Key Laboratory of High-Temperature Structural Materials & coatings Technology, Ministry of Industry and Information Technology, Beihang University, Xueyuan Road, No. 37, Beijing 100191, PR China*

[c]*School of Materials Science and Engineering, Beihang University, Xueyuan Road, No. 37, Beijing 100191, PR China*

[d]*The Institute of Advanced Manufacturing and Engineering, Faculty of Engineering, Environment and Computing, Coventry University, Coventry, CV6 5LZ, UK*

[*]Corresponding author. E-mail address: liangyf@skl.ustb.edu.cn

Abstract

This paper reports the microstructural degradation of the high Nb-TiAl alloy during the fabrication process by electron beam melting (EBM). The lamellar structure of as-EBM samples in the bottom part of the build shows significant microstructure degradation, resulting in deterioration of tensile properties at both ambient and high temperatures. Microstructural analysis has been conducted by electron back-scattered diffraction and transmission Kikuchi diffraction microscopy. Results show that the degradation of the lamellar structure is not only caused by the coarsening under the high-frequency thermal cycling during the fabrication of following layers but also attributed by the discontinuous dynamic recrystallization of the unstable initial lamellar structure due to the rapid solidification.

Keywords: Additive manufacturing; Electron beam melting; Titanium aluminide; Microstructure evolution

1. Introduction

Advanced alloy developments for high-temperature applications in the aerospace industry are primarily driven by decreasing CO_2 emissions through weight reduction and by improving high-temperature performance of engine components [1]. γ-TiAl are novel light-weight structural materials for applications up to ~800°C. Currently, the promising fields for the use of this high-performance materials are mainly for automotive engines that include valves and turbocharger turbine wheels and aero-engines that include blades and vanes, because of their low density, high specific strength, good high-temperature oxidation resistance and creep resistance [2, 3]. Long-term microstructure stability of TiAl alloy has attracted many research efforts over the past few decades. For instance, Hu et al. [4] reported that the dissolution of α_2 lamellae was accompanied by the formation of γ lamellae within it during thermal exposure. In addition, a large amount of Nb addition causes the retaining of ordered β (B2) phase at ambient temperature. The eliminated B2 phase under heat treatment would precipitate again as ordered B2 and ω phases during the long-term thermal process [5-8]. In addition, the coarsening of colony boundaries, in the form of precipitation of coarse γ and B2 phases, is found to be a common phenomenon in cast-TiAl alloy during thermal cycling experiment [9].

Compared to subtractive manufacturing methods, EBM has its inherent advantages, such as unrivalled design freedom and short lead times, which makes it suitable for the applications in automotive and aircraft engine industry [10]. Due to the use of high-speed scanning defocused electron beam and the good heat storage capability of the powder bed, EBM can operate with a high build temperature, thereby reducing the cooling rate during the solidification of the molten layers. As a consequence the resulting residual stress tends to be relatively small, in particular when comparing with the other types of additive manufacturing methods. During the fabrication of TiAl alloy, the build temperature is maintained above 1100°C, higher than its ductile-brittle transition temperature. However the solidified part has to suffer from being exposed to a relatively high temperature, above the typical service temperature of TiAl alloy. In fact, every molten layer was exposed to such a high temperature, with the first layers experienced more thermal cycles than the last ones. This may

cause mechanical property degradation and the presence of a graded microstructure and mechanical property along the building direction. The time for EBM fabricating a full-dense sample with a typical geometry of 30 × 30 × 30 mm^3 would be 5-10 hours. For the application of low-pressure turbine blades, due to their large sample height, the EBM build time would be significantly increased. It is worthwhile to mention that the lamellar structure was found to be unstable even at a temperature as low as 700°C [11]. This indicates that the microstructure stability of TiAl alloy processed by EBM would be not easy to be guaranteed. This could be attributed to the presence of Type II residual stresses [12] after the final cooling due to the difference in thermal expansion coefficients between γ and α_2 phases [13, 14].

2. Experimental

A rapidly solidified γ-TiAl based pre-alloyed powders with a nominal composition of Ti-45Al-8Nb was used for EBM fabrication (Arcam A2XX). The computer controlled electron beam scanned the layered powders in predefined patterns: the first pattern for pre-heating the entire building area to keep the temperature of the start plate at 1150°C and the second pattern for consolidating the desired areas into solid and dense metal part. The whole part was built up layer-by-layer. The dimension for each EBM sample is 30 × 30 × 30 mm^3. The EBM fabrication time was approx. 7 hours for one batch (4 samples in total).

The preheating process was employed to maintain the powder bed temperature within the range that was required to continue a stable EBM building process. The build temperature of the EBM system was measured by the thermocouple that had been attached to the start plate. The melting parameters were chosen to produce line energies ranging from 550 J/m to 400 J/m for samples 1 to 4 respectively. Four steps are included for a typical EBM building process: (i) laying powder layer, (ii) preheating, (iii) melting, and (iv) lowering the platform. Within these four steps, only the preheating process can improve the system temperature. During the four steps for each layer, the temperature fluctuation was about 100°C. In fact, the actual temperature of the bottom part of the EBM-built was expected to change more heavily. With the progress of the EBM built-up process, the building temperature that

indicates the temperature profiles of the first EBM-built layers decreased gradually from the initial 1150°C. The average temperature drop was measured to be 80°C per 10 mm.

A nearly 100% dense and crack-free EBM-built TiAl alloy was obtained by the optimised processing parameters. The presences of porosity and oxygen pick-up were observed in the initial 0.5 mm EBM build. This is likely to be due to the contamination from the start plate and the residual moisture within the EBM build chamber. As a result, EBM-built samples extracted from the initial 1 to 2 mm distance from the start plate are not considered in the present work. It is also worthwhile to note that the Al element evaporation caused by EBM processing with optimised parameters was found to be less than 0.6 at.%. In addition, the oxygen content was measured to be 810 ppm for as-EBM samples (except for the initial 0.5 mm build height) compared to 690 ppm for TiAl powders. While the nitrogen pick-up is limited in EBM process.

A Carl Zeiss Supra 40 VP field emission scanning electron microscope (SEM) was used to observe the microstructure of as-EBM TiAl samples. Crystal orientation maps were obtained using electron back-scattered diffraction (EBSD) and transmission Kikuchi diffraction (TKD). The post-EBM samples were cut by wire electrical discharge machining (WEDM) to obtain horizontal cross-sections (i.e. perpendicular to the build direction). They were then ground and polished according to standard procedures for metallographic examinations [15]. The cross-sections were made with every 5 mm in height so that the microstructure changes along the EBM build direction can be studied. The percentage of lamellar colony for each building parameters was analysed from SEM images that were collected from 10 different positions at each cross-sectional plane. The tensile properties at both room and high temperatures were investigated by using samples that had been extracted by WEDM from different heights of the EBM build block, Figure 1a. The gauge length of these tensile specimens is 10mm, Figure 1b. The surfaces of each tensile test specimen was ground with 400 to 1200 grit SiC papers prior to testing.

3. Results and discussion

Figures 2a and 2b illustrate the microstructural difference between the top part (25 mm build height) and bottom part (5 mm build height) of the as-EBM TiAl samples. The higher magnification SEM image in Figure 2c shows the presence of coarsening of the lamellar structure and the growth of equiaxed γ. In addition, Figure 2d shows that the percentage of the lamellar colony is decreased with the reduced build height. This is likely to be a result of long-term thermal cycling after the initial solidification. With the reduction of the tested build height (i.e. prolonged thermal cycling time), the rate of decline in the percentage of the lamellar colony was found to be very similar for the four samples with different EBM line energy ranging from 550 J/m (sample 1) to 400 J/m (sample 4), Figure 2d. In addition, different characteristic microstructures (i.e. fully-lamellar, nearly fully-lamellar, duplex and nearly-gamma microstructures) can be obtained by varying EBM line energies.

From the thermal cycling experiments up to hundreds of hours with the aim to study the service performance of cast-TiAl alloys, the common phenomenon was found to be the degradation of the $\gamma+\alpha_2$ lamellar colony. The present EBM work was carried on an Al-lean, high Nb-containing TiAl alloy which should exhibit better lamellar microstructure stability. However, the presence of severe dissolution of α_2 lamellae has been observed in the present work, as shown in Figures 2b and 2c. Such an effect could not be removed by the different EBM building parameters adopted here. It is also important to note that the actual Al content was measured to be 44.5 at.% in the as-EBM samples, indicating that the Al evaporation was not significant and thereby a similar amount of α_2 phase would be expected within the lamellar colony grains. Thus the evolution of microstructure in the EBM built sample should not be solely attributed to the long-term thermal cycling. Here we postulate that the microstructural degradation could be due to the rapid solidification induced by EBM process and the intrinsic thermodynamic instability of $\gamma+\alpha_2$ lamellar structure. This seems to be consistent with the existing knowledge in physical metallurgy of TiAl alloy. When a fully lamellar structured TiAl alloy is fabricated by casting followed by the heat

treatment, the microstructure optimisation is normally carried out by first heating the cast-TiAl to the single α-phase field, then furnace cooling through the (α+γ) phase field. This leads to the final phase compositions being far from thermodynamic equilibrium state [17, 18]. This provides a driving force for thermal instabilities of the lamellar microstructure and hence leads to the dissolution of α_2 lamellae and dynamic recrystallisation [17, 19].

Three types of grain boundaries based on their misorientation angles were found in the present EBM-built samples. As shown in Figure 3, these grain boundaries include low angle grain boundaries from 2°-10° (LAGBs), medium angle grain boundaries of 60° or 70° (MAGBs) and high angle grain boundaries of 87±3° (HAGBs). The cyan lines represent LAGBs, while the red lines represent 60º<111> pseudo and 70º<110> true twin boundaries of γ phase. These twin boundaries were believed to act as ideal sites for dynamic recrystallisation nucleation, especially for discontinuous dynamic recrystallisation (DDRX) [20]. The black lines illuminate the HAGBs of 87±3° which are caused by dynamic recrystallisation and grain coarsening through consumption of the neighbouring grains. The twin boundaries (60° or 70° misorientation angles) appear to be within the coarse γ grains and on the gamma grain boundaries, while the 87° grain boundaries are widely distributed in the γ grains, Figure 3a. Figure 3c shows the lamellar structure in the as-EBM TiAl alloy. Grain boundaries with misorientation angles of 89° were present at both the initial fine lamellar structure and the coarsened lamellar microstructure, Figure 3c. Figures 3b and 3d are the inverse-pole-figure (IPF) orientation maps of as-EBM TiAl alloy. The large density of HAGBs appearing in the coarsened lamellae indicates that lamellar degradation in EBM process is closely related to DDRX [20, 21].

Figure 4a shows the distribution of grain misorientation angles at different EBM-built height, from which the mechanical test samples were extracted. With the decreasing sample height of the EBM-built, the TiAl alloy experienced a longer period of temperature fluctuation. This accounts for the highest percentage of HAGBs and the lowest percentage of twin boundaries in the EBM sample at the height of 5mm, Figure 4a. It can be also seen in Figure 4a that 90% of grain boundaries were HAGBs (~89° misorientation angles) and there was no grain boundaries with misorientation

angles of 10-15°. This indicates that the main dynamic recrystallisation mode in long-term EBM process is DDRX instead of the continuous dynamic recrystallisation (CDRX), which is associated with the accumulation and tangle of dislocations [20]. Due to the rapid cooling process, the microstructure instability of the initial lamellae is also more severe. Together with the subsequent repeated thermal cycling resulting from the next built layers, residual stresses introduced as a result of the thermal mismatch of elastic modulus and thermal expansion between γ and α_2 phases can further accelerate the microstructure degradation. As described in [13] this can affect the kinetics of DDRX.

Figure 4b shows the mechanical testing data of EBM-built TiAl alloy at room temperature (RT), 800°C and 900°C, as well as the Hot-Isostatic-Pressing processed (HIPped) TiAl alloy tested at RT. The TiAl sample that had been extracted from the lowest EBM sample height had the smallest σ_b at 900°C, see green colour columns in Figure 4b. There was insignificant variation of σ_b at 900°C for samples that had been extracted from the other EBM sample heights, Figure 4b. A similar trend can be observed for σ_b at 800°C, see blue colour columns in Figure 4b. Compared to these high temperature results, σ_b at the room temperature of EBM-built TiAl samples did not show any obvious dependency on the sample height; the sample that had been extracted from the lowest EBM build height had the smallest σ_b, Figure 4b. This could be due to the occasional presence of EBM processing induced defects such as pores and micro-cracks. Some level of improvement in room temperature σ_b can be achieved by subjecting the EBM-built samples to the HIPping process, as shown in Figure 4b particularly for 23 mm and 27 mm sample heights. As also shown in Figure 4b, the magnitude of σ_b for the HIPped TiAl samples reduces with the decrease in the EBM sample height. The dependency of the tensile strength on the EBM build height could be related to the microstructural degradation. The decomposition of α_2 phases might be the most important factor attributing to the property reductions. The exposure-induced embrittlement phenomenon (700°C in air) associated with the decomposition of $\alpha 2$ phases in both cast and cast+forged TiAl alloys was reported by Huang and Cong [22].

The tensile ductility at room temperature of the present EBM-built TiAl alloy was

found to be less than 0.5%. Considering the fine lamellar microstructure as shown in Figure 2, such a low ductility is not in the expectation. The ductility of γ-TiAl alloy has been recognised to be sensitive to lamellar spacings, and thereby fine lamellar structures are considered to be beneficial for the property [23]. In addition, less than 0.5 at.% Al evaporation and little micro-segregations were confirmed in the EBM-built samples. Thus it is most likely that the low room temperature ductility is due to the destruction of lamellar interfaces, the fracture of α_2 phases and the coalescence of neighbouring γ lamellae, as previously suggested in [22] for thermally exposed cast and cast+forged TiAl alloys.

EBM processing has been used to fabricate high Nb-TiAl alloy. Compared with the traditional casting method [24], EBM-built TiAl alloy exhibits a fine-lamellar microstructure. This is because that the rapid solidification can be achieved by the very local heat input and the small volumes of molten material. In addition, the large coefficient of thermal conductivity between the solid and the liquid results in the fact that the rate of solidification during the EBM process is 1-2 orders of magnitude higher than that of the quenching. The apparent refinement effect and restraint of segregation via EBM process make the mechanical properties of TiAl alloy higher than those of casting produced TiAl alloy. It is important to note that the use of EBM to fabricate TiAl alloy might avoid of employing complex post-EBM heat treatment procedure. This will help to prevent falling into the classic dilemma in cast-TiAl, which is the elimination of the brittle β (B2) phase by long-term thermal soaking at single α-phase field and the prevention of unwanted growth of α phase by reducing the thermal soaking time. In terms of the EBM processing, this work shows that the degradation of the γ+α lamellar colony could occur due to their thermodynamically unstable state. The microstructure degradation could be minimised by optimising the chemical composition (for example increasing content of Nb) and the EBM building parameters (for example decreasing the temperature fluctuation).

4. Conclusion

The microstructural degradation that includes the coarsening of lamellae and growth of equiaxed γ grains was found on the EBM-built TiAl alloy. Room temperature

tensile strength on the HIP processed EBM-TiAl samples increased with the increasing sample height of the EBM-built. Such mechanical property dependence on the sample height is likely to related to the microstructural degradation. The microstructural degradation of the lamellar structure is not only caused by the coarsening under the repeated thermal cycling but also attributed to the DDRX of the unstable initial lamellar structure that formed as a result of rapid solidification over the EBM process.

Acknowledgements

This research was supported by the National Natural Science Foundation of China (No. 51671016). Bo Chen acknowledges financial supports by the UK's Engineering and Physical Sciences Research Council, EPSRC (EP/P025978/1) and Coventry University through the Early Career Researcher – Outgoing Mobility Award to facilitate this international research collaboration.

References

[1] Y. W. Kim, Symposium on Gamma Titanium Aluminides, at the TMS 95 Annual Meeting, 637(1995).

[2] F. Appel, U. Brossmann, U. Christoph, U. Eggert, P. Janschek and J. Paul, Adv. Eng. Mater. 2, 699 (2002).

[3] Y. W. Kim, JOM 41, 24(1989).

[4] D. Hu, A. B. Godfrey and M. H. Loretto, Intermetallics 6, 413(1998).

[5] X. Du, J. Zhu, X. Zhang, Z. Cheng and Y. W. Kim, Scr. Mater. 43, 597(2000).

[6] Z. Huang, Intermetallics 37, 11(2013).

[7] L. Zhou, V. Lupinc and J. T. Guo, Mater. Sci. Eng. A 354, 97(2003).

[8] Z. Huang, W. Voice and P. Bowen, Scripta Mater.48, 79(2003).

[9] D. B. Williams, E.P. Butler, Inter. Metals. Rev. 26, 153(1981).

[10] J. Kranz, D. Herzog and C. Emmelmann, J. Laser Appl. S14001, 27(2015).

[11] T. Cheng, Intermetallics 995, 7(1999).

[12] B. Chen, P. E. J. Flewitt, A. C. F. Cocks and D. J. Smith, Int. Mater. Rev. 1, 60(2015).

[13] W. Zhao, Y. Pei, D. Zhang, Y. Ma, S. Gong and H. Xu, Intermetallics 429, 19(2011).

[14] H. Jiang, T. Rong, D. Hu, I. P. Jones and W. Voice, Intermetallics 1433 14(2006).

[15] S. Xu, X. Xu, Y. Xu, Y. Liang and J. Lin, Mater. Des. 101, 88(2016).

[16] L. Fang, J. Lin and X. Ding, Mater. Chem. Phys. 112, 167(2015).

[17] T. Parthasarathy, M. Keller and M. G. Mendiratta, Scr. Mater. 1025, 38(1998).

[18] A. Chatterjee, H. Mecking and E. Arzt, Mater. Sci. Eng. A 840, 329(2002).

[19] S. Bystrzanowski, A. Bartels, H. Clemens, R. Gerling, F. P. Schimansky, G. Dehm and H. Kestler, Intermetallics 515, 13(2005).

[20] Y. Zong, D. Wen, Z. Liu, and D. Shan, Mater. Des. 321, 91(2016).

[21] H. Niu, Y. Chen, Y. Zhang, J. Lu, W. Zhang and P. Zhang, Mater. Des. 196, 90(2016).

[22] Z. Huang, T. Cong, Intermetallics 18, 161(2010).

[23] K. S. Chan and Y. W. Kim, Acta Metall. Mater. 439, 43(1995).

[24] D. Herzog, V. Seyda, E. Wycisk and C. Emmelmann, Acta Mater. 371, 117(2016).

Manuscript

Click here to download Manuscript List of figures and tables_Kan_20170810.docx

Click here to view linked References

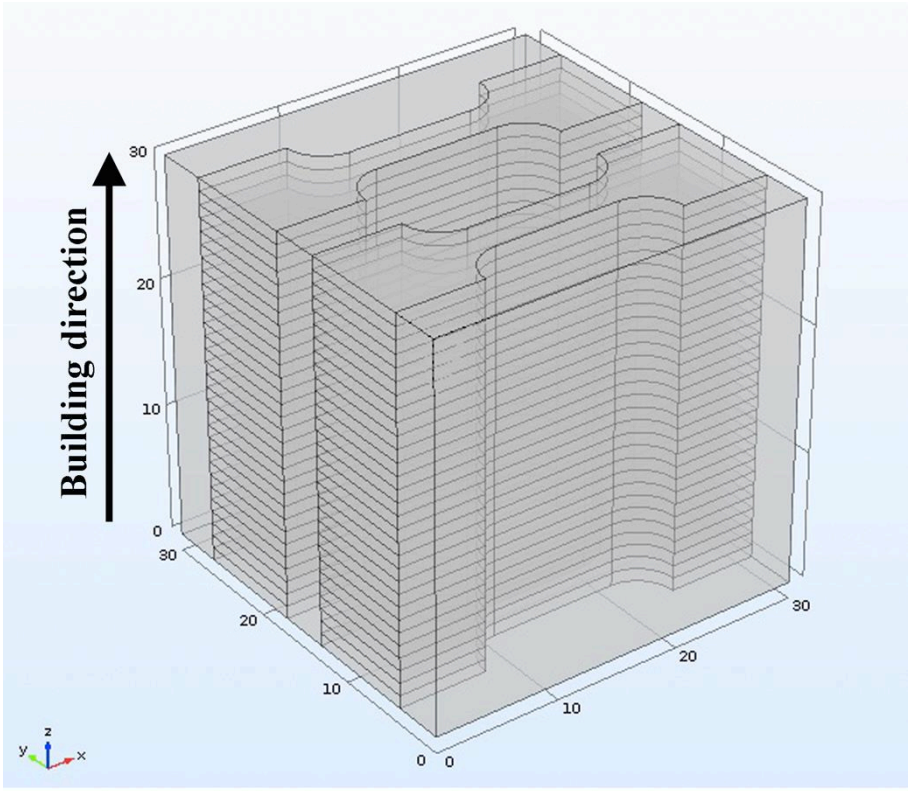

(a)

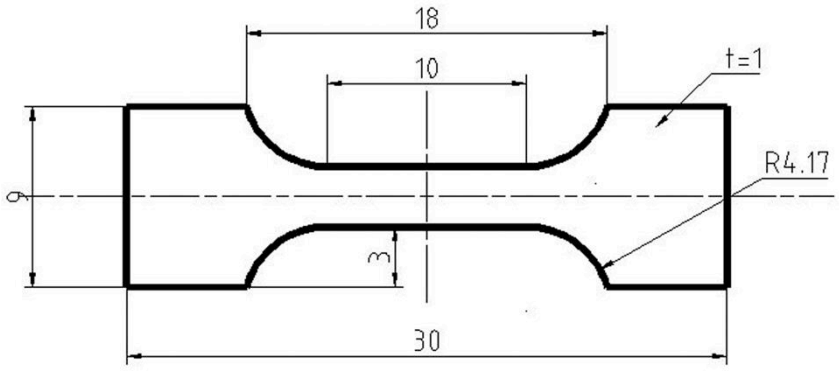

(b)

Figure 1: (a) 3D schematic of tensile test specimens that were extracted by WEDM from different heights of the EBM-built block, (b) the dimension of tensile test specimen with a 10 mm gauge length and 3 mm gauge width.

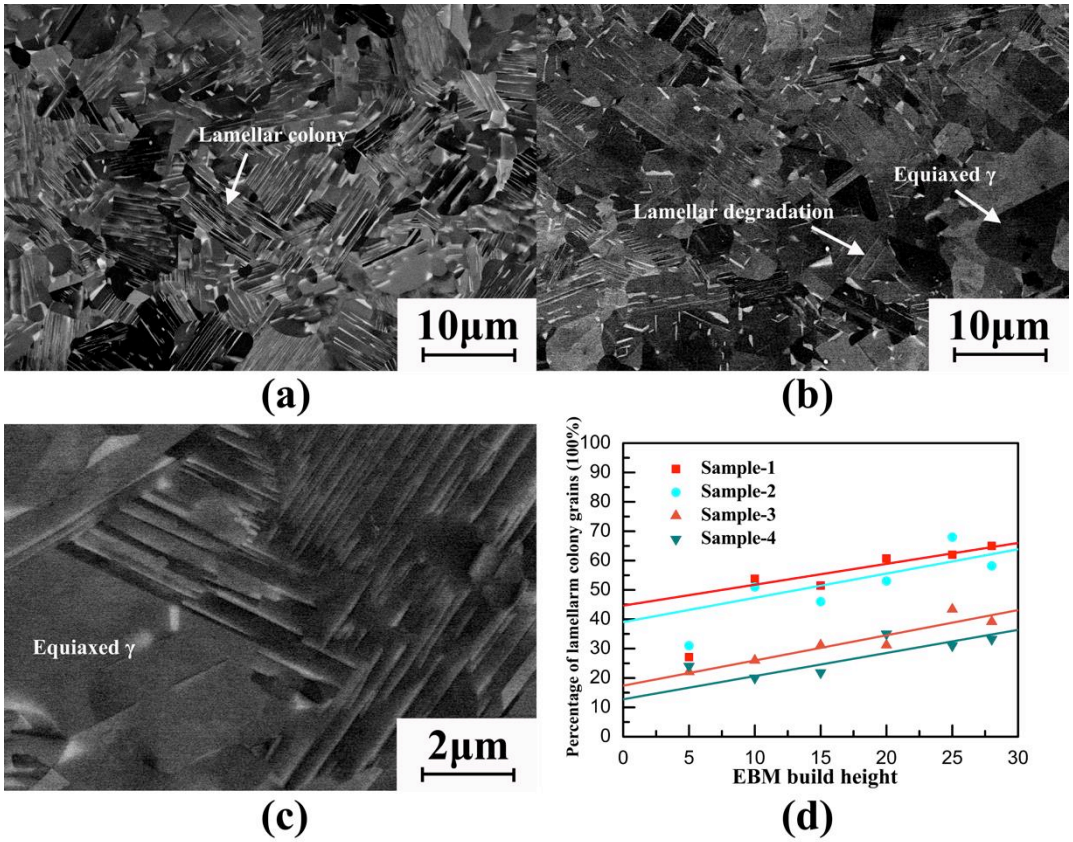

Figure 2: (a) the microstructure of as-EBM TiAl sample at the build height of 25mm, (b) and (c) the microstructure of as-EBM TiAl sample at the build height of 5mm, (d) the percentage of lamellar colony grains changing with different build height. Note: the energy input during the EBM fabrication for samples 1 to 4 were 550, 500, 450, 400 J/m, respectively.

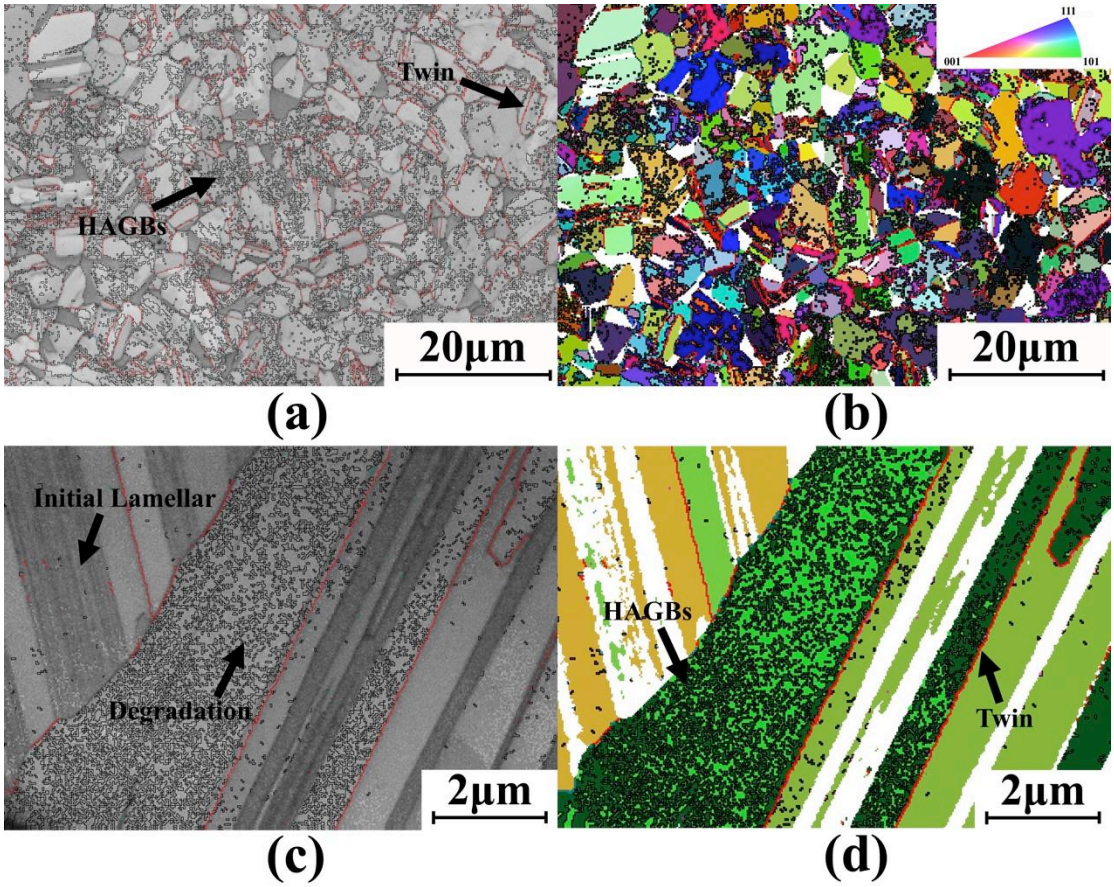

Figure 3: (a) and (c) are transmission Kikuchi diffraction (TKD) band contrast maps, (b) and (d) are TKD inverse pole figure orientation maps of as-EBM TiAl alloy. The red lines and black lines represent γ phase twin boundaries (60° and 70°) and HAGBs of 87±3°, respectively.

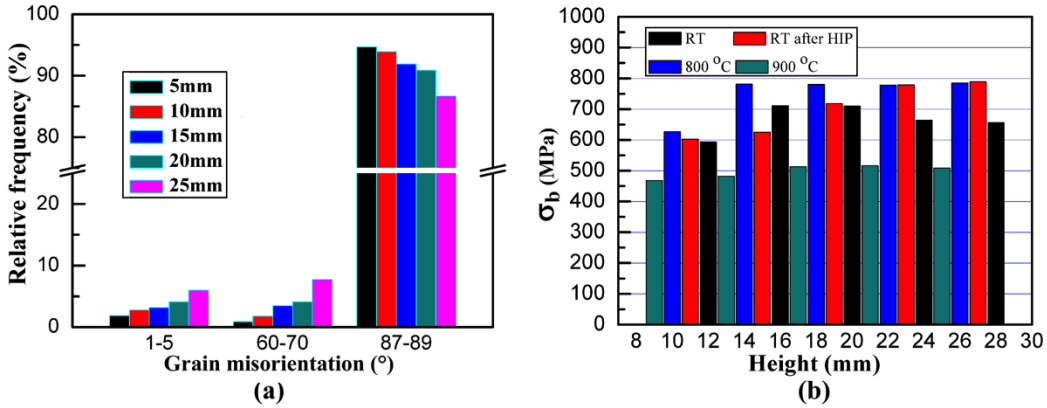

Figure 4: (a) The relative frequency of grain misorientation from different build heights of the as-EBM TiAl samples, (b) the ultimate tensile strength (σ_b) of the as-EBM and HIPped samples tested at the room temperature, as well as the as-EBM samples tested at 800°C and 900°C. Note: The higher σ_b at 800°C and 900°C compared to σ_b at the room temperature was due to the room temperature low ductility (i.e. the TiAl sample failed before reaching to the yield point at the room temperature)

Figure

Click here to download Figure fig. 1.tif

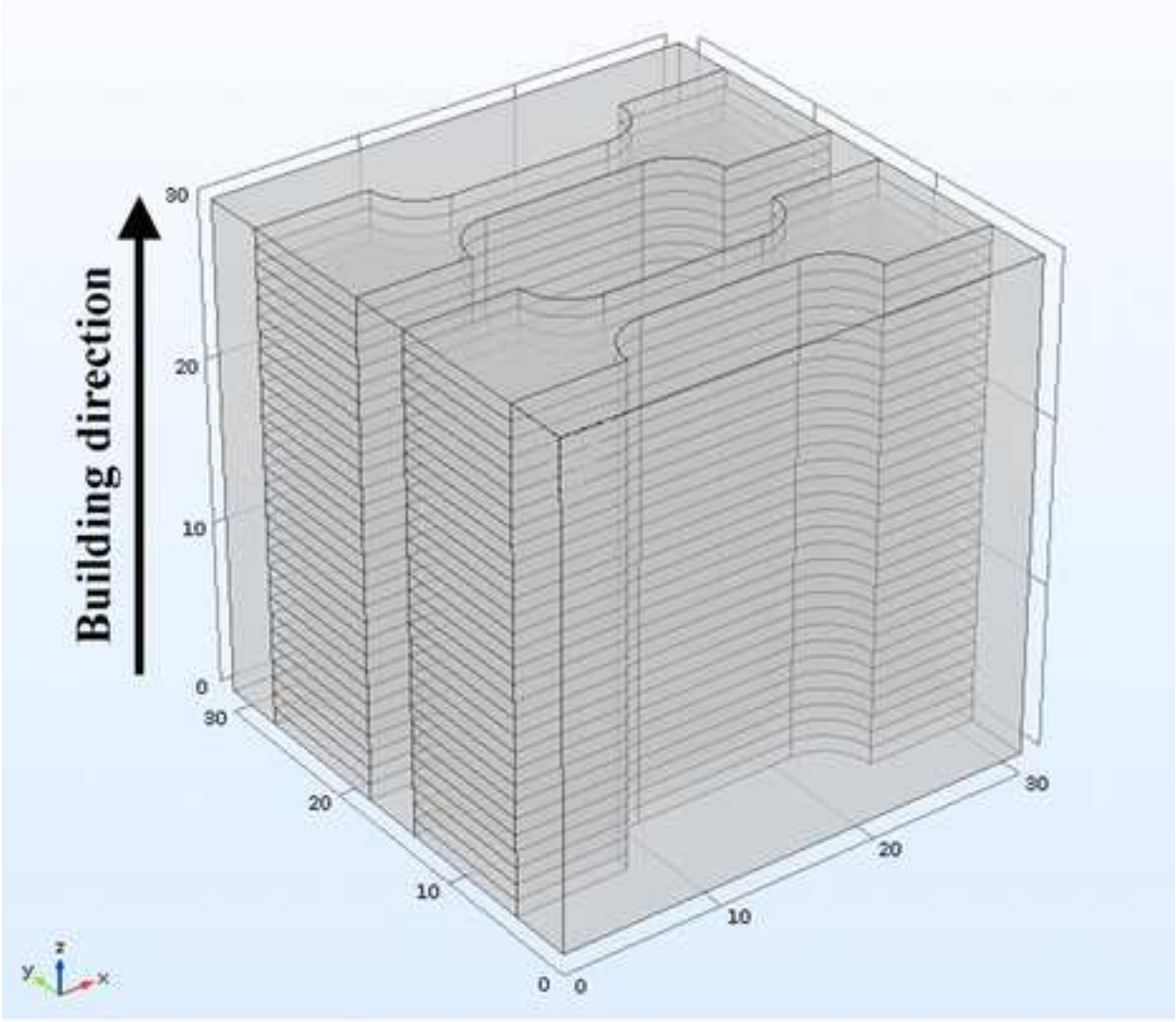

(a)

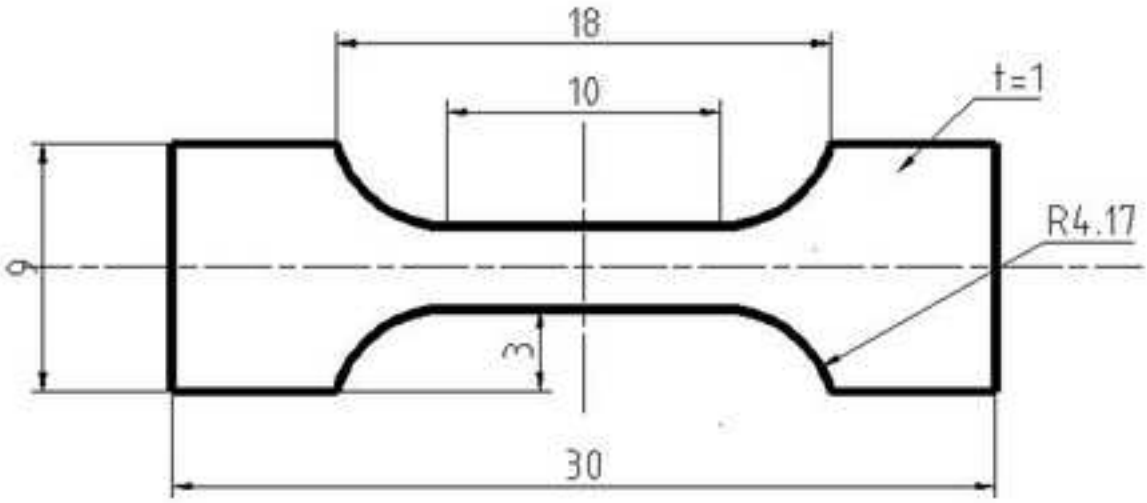

(b)

Figure

Click here to download Figure fig. 2.tif

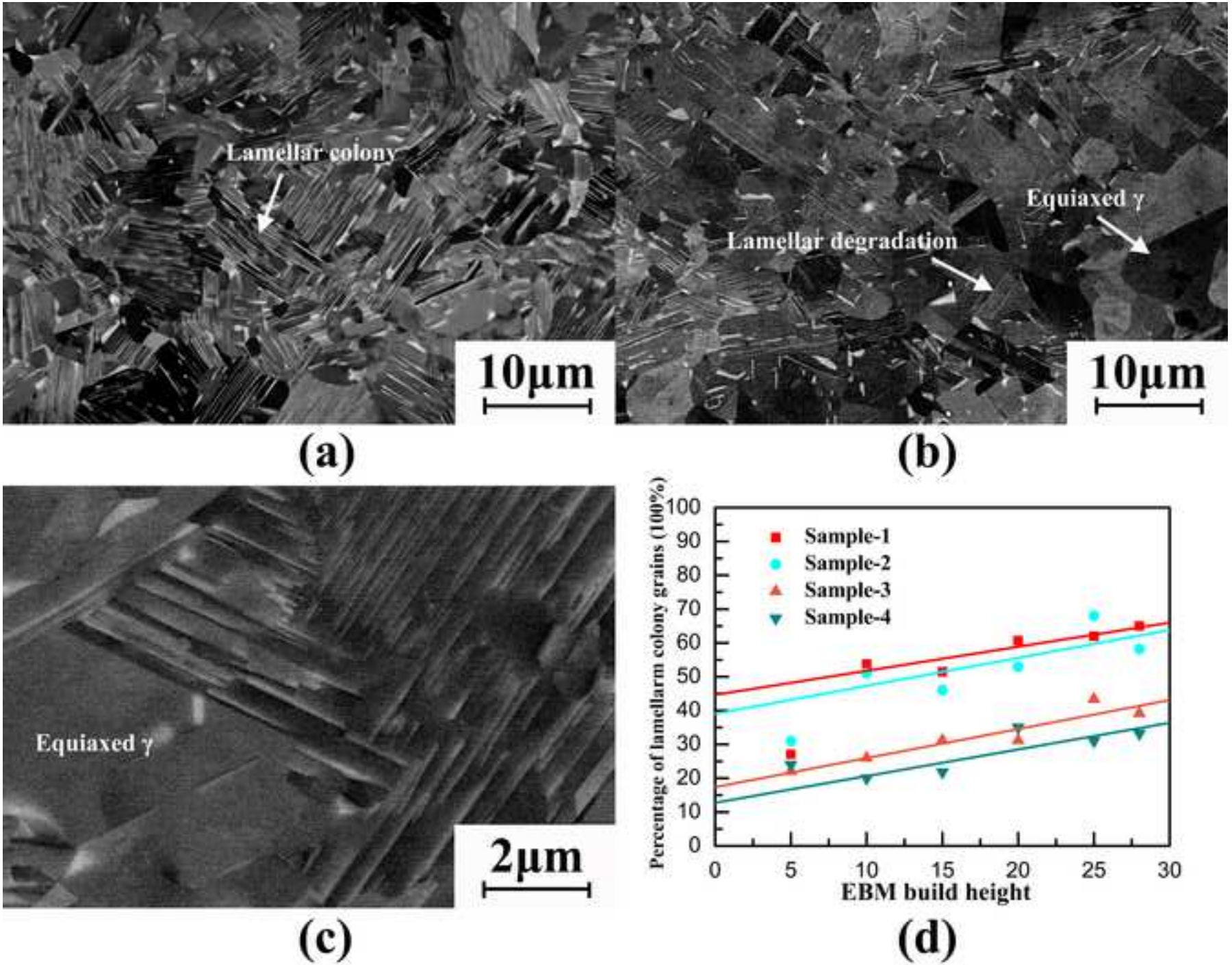

Figure

Click here to download Figure fig. 3.tif

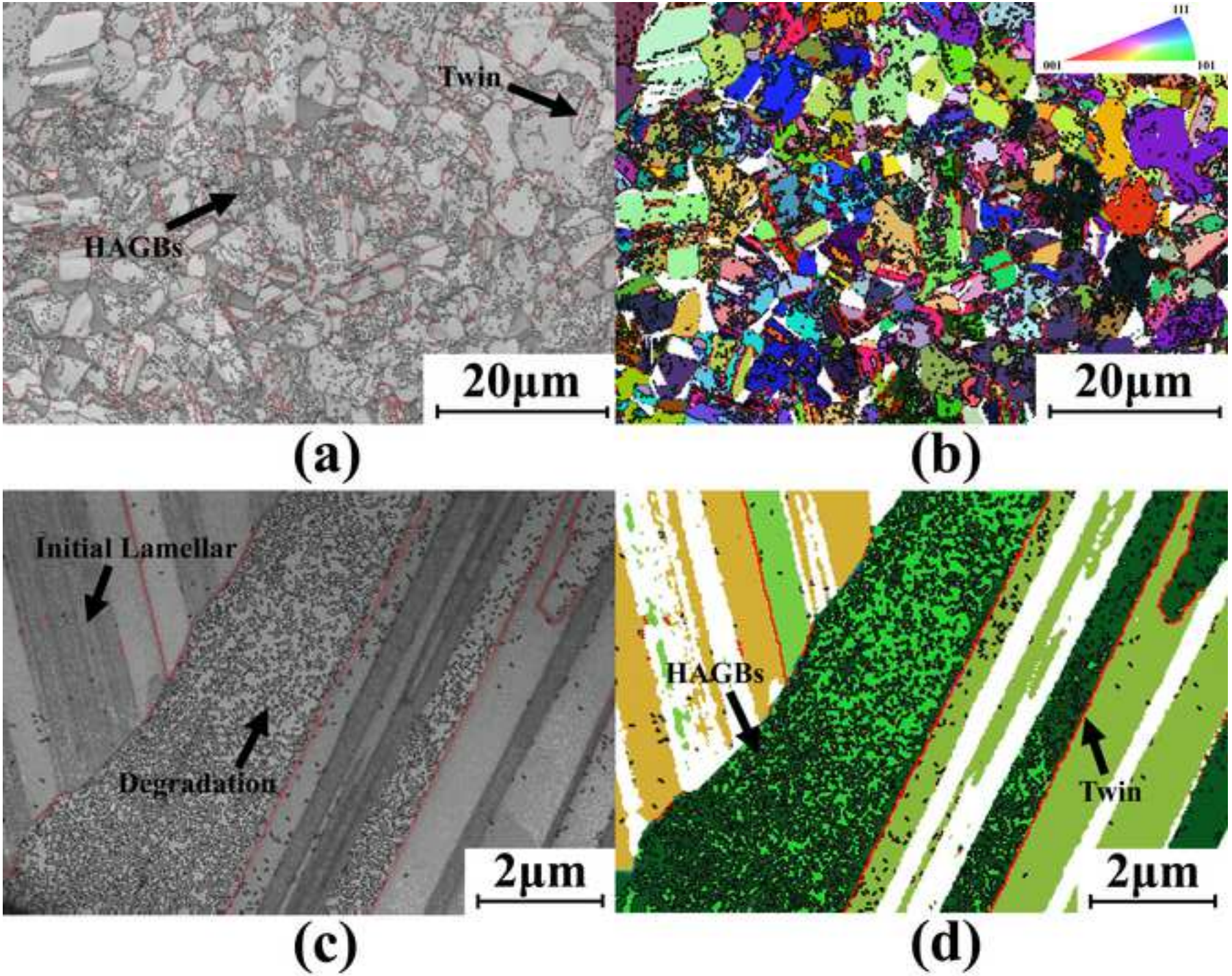

Figure

Click here to download Figure fig. 4.tif